Springer

KSME

Journal of Mechanical Science and Technology 31 (6) (2017) 2933~2941
www.springerlink.com/content/1738-494x(Print)/1976-3824(Online)
DOI 10.1007/s12206-017-0536-z

Modeling and flow analysis of piezoelectric based micropump with various shapes of microneedle †

Rakesh Kumar Haldkar*, Vijay Kumar Gupta and Tanuja Sheorey

PDPM Indian Institute of Information Technology Design and Manufacturing Jabalpur, 482005, India

(Manuscript Received October 22, 2016; Revised February 3, 2017; Accepted February 23, 2017)

Abstract

Micropumps have been investigated as drug delivery and disease diagnostic devices. Many of these micropumps have been designed, considering primarily, available micro fabrication technologies rather than appropriate pump performance analysis. Piezoelectric and silicon based micro pumps are more popular as compared to other smart materials being explored. The microneedle is an integral part of these micropumps providing an interface between the drug reservoir and the patient's body for extracting the blood for investigation. Blood collected in the pump chamber passes through the biosensor and gives the required investigation report. It is aimed to minimize the pain while the microneedle is inserted in the body without having any effect on the flow characteristics. Several factors affect the pain while inserting the needle, out of which shape and size of the microneedle are two important parameters. In this study we have investigated the effect of shape of the microneedle on the flow inside the micropump. A micropump design is based on the required flow at the biosensor point. All computations were carried out with water (Newtonian fluid) as the working fluid after carrying out a comparative analysis with human blood (non-Newtonian fluid). For the pentagonal shaped microneedle, the velocity at the top of the microneedle was minimum, which is beneficial in that fluid should remain in contact with the sensor for longer time.

Keywords: Microneedle; Micropump; Piezoelectric bimorph; Pressure; Velocity

1. Introduction

Micropumps have been investigated for drug delivery and disease diagnostic devices. For collection of blood sample, a microneedle is inserted into the body. The microneedle acts as an interface between the micropump and the human body. Pain is felt when the needle is inserted in the body; therefore, needle size should be as small as possible. Tsuchiya et al. [1] reported that human beings do not feel pain when a mosquito inserts its labrum, which has the equivalent needle size of approximately 60 μm. Also, they studied the effect of the shape of the microneedle on pain and concluded that pentagon shape gives minimum pain.

Microneedles are classified into three categories: solid, hollow, and dissolvable. In the present study, we considered hollow microneedles of inner diameter 100 μm. Various materials such as titanium, metals, polymers, and silicon have been explored for fabrication of microneedles [2-5]. Several tip geometries like a volcano, snake fang, micro-hypodermis are reported in the literature for microneedles [6]. The body or shaft of microneedles, however, was formed into simple shapes such as cone, cylinder, bevel or pyramid. Other geometries such as extremely sharp and side-open microneedles have also been reported in the Ref. [7].

Li et al. [8] introduced an ultra-high-aspect (2 mm length and 60 μm inner diameter) microneedle in a polydimethylsiloxane elastic self-recovery actuator. They studied the liquid extraction ability of a micro-pump system and optimized microneedle for minimally invasive blood extraction. They observed that when the inner diameter of the microneedle is 100 μm, bevel angle does not have any effect on extraction time [9, 10].

The shape of the microneedle affects pain, insertion force and flow of fluid. Blood extraction system based on the concept of female mosquito's blood sampling mechanism was developed and effectiveness of the pumping system was evaluated [1]. Gupta et al. [11] studied the effect of microneedle insertion depth, needle retraction, and infusion flow rate on associated pain and observed that shorter needle and slower flow rate results in low pain. An array of microneedles was used for drug delivery in a non-painful manner, and size of microneedle was decided based on the anatomy of the skin [12]. Cohen and Chang [13] studied the effect of design parameters such as pump geometry, material and operating modes on the volume of chamber that is available between the peaks and

*Corresponding author. Tel.: +91 761 2794413
E-mail address: rakeshhaldkar@gmail.com
† Recommended by Associate Editor Seong-Chan Jun

valleys of the waves. Performance of a piezoelectrically actuated valveless micropump with consideration of the three-way electro-mechanical-fluid couplings using FEM was analyzed by Bin et al. [14]. Simulation results showed that the pumping efficiency depends not only on the actuating frequency and maximum magnitude of the membrane deflection, but also on the deflected shape of the membrane. Ha et al. [15] investigated pumping performance of a piezoelectric valveless micropump in terms of three-dimensional electro-fluid-structural interaction. ANSYS and ANSYS CFX were used for the structural and fluid domains, respectively. The authors developed and investigated a wearable human blood sampling system without a centrifugal separator and large-sized blood sampling system as in conventional glucose level monitoring systems. Their design was based on the concept of a female mosquito's blood sampling [16]. Thorat and Patil [17] studied the performance of a reciprocating pump using CFD [17]. The analytical model helps to improve the microneedle design by minimizing the pain of insertion and increasing the mechanical strength; the conclusion was that the fluctuation of the flow rate decreases with the increase in frequency [18, 19].

Our focus was to achieve the required flow for sensing, which is of the order of few microliters. For the same, flow analysis inside the microneedle and pump chamber with various shapes of the microneedle namely circular, pentagon, and octagon was carried out. Velocity and pressure conditions at specific locations in the fluid region were analyzed in detail using ANSYS and ANSYS-CFX to obtain appropriate needle shape as per the required flow at the biosensor location.

2. Piezoelectric micropump

To analyze effect of shape of the microneedle on the fluid flow, micropump developed by Tsuchiya et al. [1] was considered and analyzed in this study. Fig. 1 shows a schematic diagram of the micropump. The micropump consists of cylindrical pump chamber in which the fluid will be collected. A biosensor is placed at the bottom of the pump chamber, 2.25 mm from the microneedle towards the outlet valve, along the same radial direction. A microneedle of length 3.8 mm and diameter 100 μm is attached at the center of the pump chamber, which acts as the inlet of the fluid. A piezoelectric ($Pb(ZrTi)O_3$ based) bimorph is attached at the top portion of the pump chamber acts as diaphragm. On application of the harmonic voltage, the piezo bimorph moves up and down in the pump chamber to create suction and pressure. The fluid is sucked inside the pump chamber through microneedle during suction, while it flows out of it during pressure. An outlet valve at the side of the pump chamber opens when the pressure inside exceeds a particular limit to throw the liquid out. The bimorph consists of two discs of piezoelectric material, glued together using silver glue. Material properties for the piezo bimorph are $d_{31} = d_{32} = -375*10^{-12}$ C/N, $d_{33} = 710*10^{-12}$ C/N, relative dielectric constant 4600 and density is 8100 kg/m^3. Material properties for stainless steel and Silver glue are summarized in Table 1.

Table 1. Material properties of silver glue and stainless steel.

Name	Density (Kg/m^3)	Poisson's ratio	Young's modulus (GPa)
Silver glue	10500	0.37	75.842
Stainless steel	7700	0.30	200

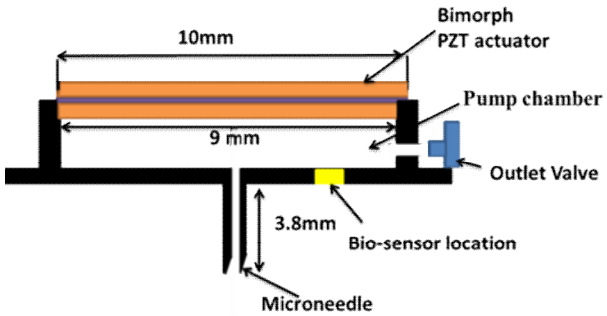

Fig. 1. Schematic diagram of micropump.

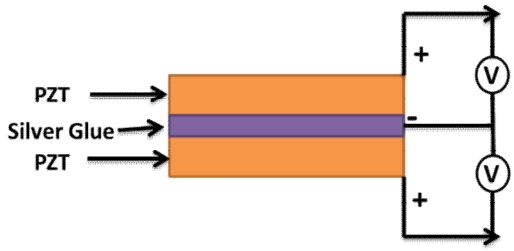

Fig. 2. Schematic diagram of PZT and silver glue.

2.1 Actuation of micropump

For actuation of the micropump, a voltage of 20 V is applied on piezo bimorph, keeping silver glue as ground (Fig. 2). On application of sinusoidal voltage, upper piezo contracts/expands and the lower piezo expands/contract, resulting in bending of the piezo bimorph, creating suction and pressure inside the chamber.

2.2 Microneedle

The purpose of the microneedle in the micropump is to suck the fluid from the reservoir and supply it in the pump chamber. The collected fluid passes over the biosensor and will be analyzed. To provide sufficient time for reaction with biosensor, the fluid velocity should be low. In this study, we analyzed flow through various shapes of the microneedle. For analysis purpose, water was considered as the fluid in place of blood. Dimensions of microneedles were chosen such that hydraulic diameter remained same for all the microneedles: 100 μm.

3. Finite element modeling and analysis

For analyzing the effect of the shape of the microneedle on the flow along its length and in the pump chamber, Ansys®12.1 was used as a tool for the simulations. The analysis involved three phases.

I. Flow through various shapes of microneedle.
II. Modal and FEA analysis of piezo actuator.
III. Flow analysis with complete setup.

3.1 Flow through various shapes of microneedle

To analyze the flow in the microneedle, only the microneedle was separately modeled and analyzed for various pressure differences. At one end of the microneedle (inlet), 100 kPa pressure was applied (which corresponds to pressure of blood inside the human veins) and at the other end (outlet) pressure was varied (25, 50 and 75 kPa). Due to the pressure difference, variation in the velocity of the fluid at the outlet of the microneedle was observed and is shown in Figs. 3(a)-(c). The observed velocities are summarized in Table 2. From the table, it can be observed that when the pressure at the outlet increases, outlet velocity reduces. Also, the shape of the microneedle has a significant effect on the outlet velocity of the fluid. Octagon and circular microneedles give more velocity compared to pentagon microneedle.

3.2 Modal and FEA analysis of piezo bimorph actuator

Natural frequencies of the piezo bimorph were observed using modal analysis. Deflection and pattern of the piezo biopump near first natural frequency was analyzed using harmonic analysis under actuation of a 20 V electric field. Next, transient analysis was used to observe flow dynamics.

Table 2. Velocity at different pressure and shapes.

Name	Velocity (m/s) at 25 KPa	Velocity (m/s) at 50 KPa	Velocity (m/s) at 75 KPa
Circular	2.080	1.391	0.6976
Octagonal	2.082	1.392	0.6981
Pentagonal	2.072	1.386	0.6954

3.2.1 FEA model

Initially, analysis was on the piezo bimorph alone. For modeling the piezo bimorph in Ansys, symmetry was explored and analysis was carried out on only half-domain as shown in Fig. 4. Piezo bimorph actuator was connected to the chamber across circular outer ring of 0.5 mm width. SOLID226 (twenty node tetrahedron) element was used for the piezoelectric actuator and SOLID186 (Twenty node tetrahedron) element was used for the silver glue. Following boundary conditions were applied on the model:

(1) Outer ring of 0.5 mm width was considered fixed along thickness direction (Uz = 0).

(2) Symmetry boundary condition on cutting plane.

3.2.2 Mesh independence test of piezo bimorph actuator

The piezo bimorph actuator was meshed with varying number of elements, ranging from 1000 to 80000. With each case, change in natural frequency was observed. Fig. 5 shows variation of natural frequency with number of elements in the actuator. Using 35000 elements, first natural frequency of 47186 Hz was observed. Increase in number of elements beyond 35000 brings deviation of the order of 0.21 % and hence was ignored.

3.2.3 Modal and harmonic analysis

First natural frequency was observed at 47186 Hz using modal analysis. For the harmonic analysis, the frequency range was set between 44000 Hz to 49000 Hz (covering first natural frequency of 47186 Hz). The maximum deflection of 3.2×10^{-6} m was obtained at the center of the piezo disc, corresponding to the natural frequency of 47186 Hz as shown in Fig. 6(a).

3.2.4 Transient analysis

For detailed transient analysis, the time period of 21.1927 µs (1/47186 Hz) was divided into 20 sub steps. The analysis was for 40 cycles for the total time of 848 µs and is plotted in Fig. 6(b). Beating phenomenon was observed near the frequency of 47186 Hz. Beating phenomenon leads to increasing

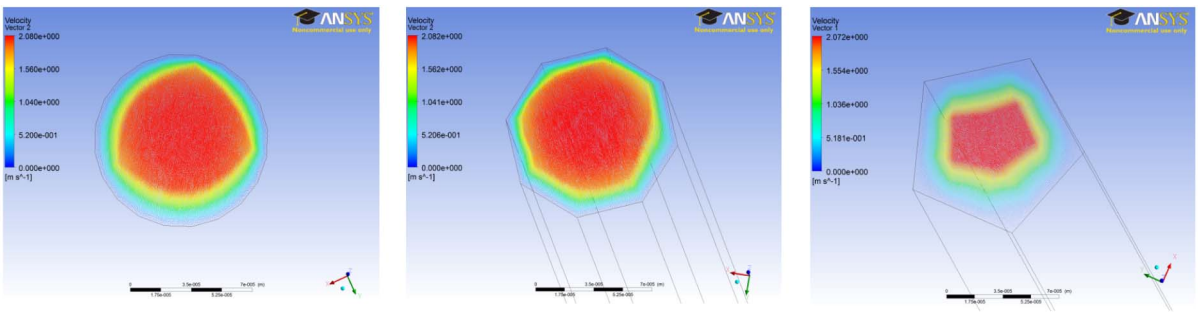

(a) (b) (c)

Fig. 3. Velocity variation in microneedle: (a) Circular; (b) octagonal; (c) pentagonal.

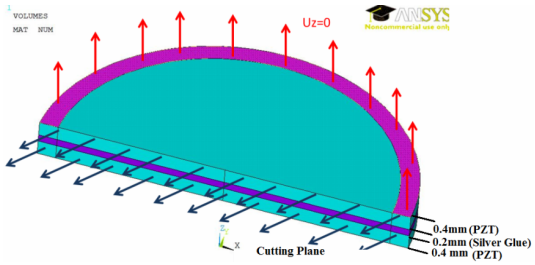

Fig. 4. Piezo bimorph.

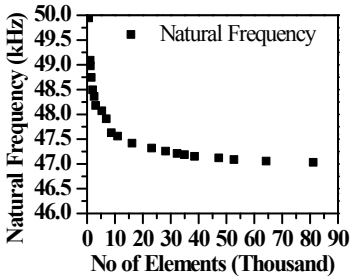

Fig. 5. Mesh independency of piezo bimorph actuator.

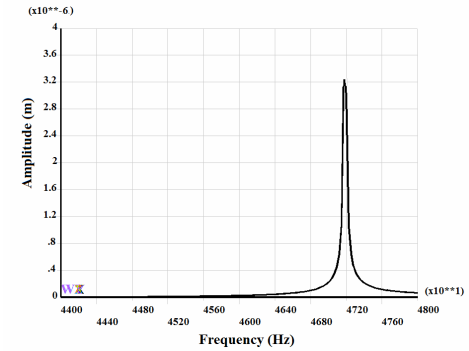

(a)

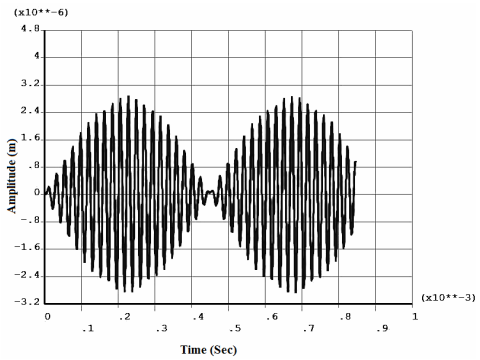

(b)

Fig. 6. Dynamic analysis of piezoelectric actuator: (a) Harmonic analysis; (b) transient analysis.

amplitude, resulting in accumulation effect.

3.3 CFX analysis of micropump

After analyzing the microneedle and piezo bimorph individually, we developed and analyzed a full model for the piezo bimorph micropump. The analysis included flow analysis in the pump parts, namely, circular microneedle, pump chamber and their interaction with each other. Analysis was on half domain considering symmetry, as shown in Fig. 7.

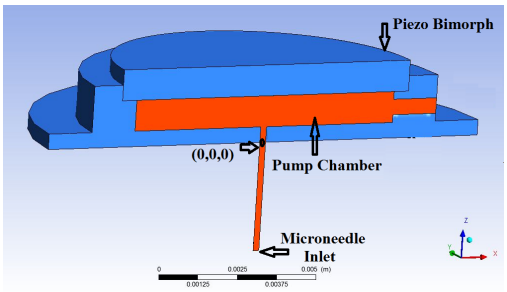

Fig. 7. Model for fluid flow analysis of pump.

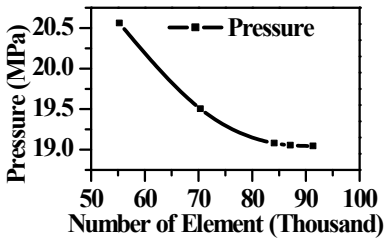

Fig. 8. Mesh independence test for pump chamber and fluid region.

3.3.1 Modeling of pump chamber and fluid region

With the addition of fluid region, mesh independence test was again carried out. Number of elements of fluid domain was varied from 50000 to 90000 and after 85000 elements the results were almost the same as depicted in Fig. 8. The pressure deviation between 87103 and 91312 elements was 0.041 %. With further refinement of mesh near the junction of the microneedle and the pump chamber, finally, 90233 elements were considered for meshing.

Figs. 9(a) and (b) show CAD and FEA model of the domain. Fig. 9(a) shows CAD model of solid regions comprised of micropump, microneedle and outlet valve and their respective fluid regions. The relative position of microneedle and the outlet valve can be seen vividly. Material for the solid region was considered as steel and meshed using SOLID186 element of Ansys® (20 node tetrahedron element). A fluid region named as "Fluid region" was developed in the pump using FLUID142 element of Ansys with MESH200 type. Fig. 9(b) shows meshing of complete assembly on which the CFX analysis was carried out.

3.4 Fluid structure interaction

Actuation of bimorph inside the micropump chamber results in the interaction of fluid surface of water and solid surface of the piezoelectric. This interaction is known as fluid-structure interaction. Applying harmonic voltage to piezo bimorph near the first natural frequency results in pumping

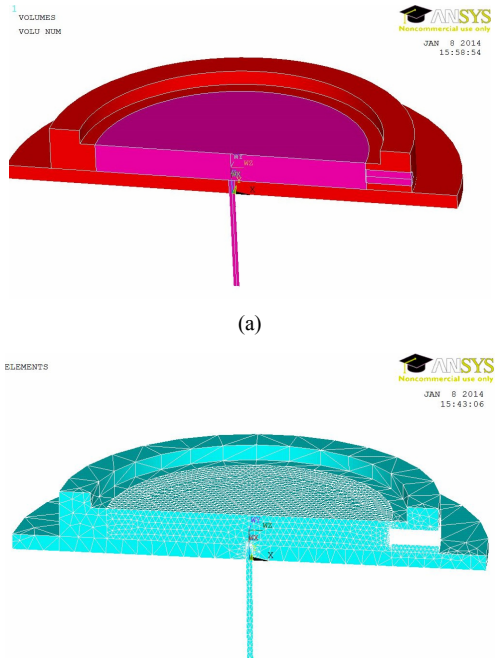

Fig. 9. FEA modeling of micropump: (a) CAD model of pump; (b) FEA model of pump.

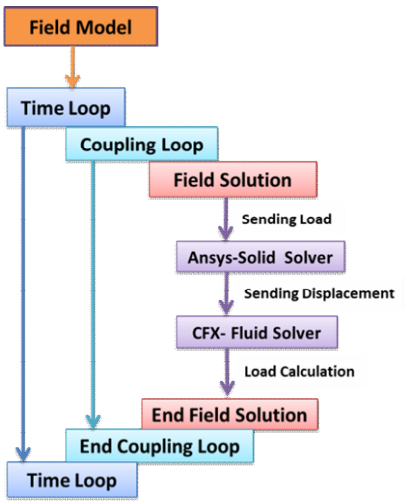

Fig. 10. ANSYS multi-field solver algorithm.

action of the micropump. The combined effect of the suction and pressure cycle of the bimorph actuator causes required flow of fluid in the device.

Two-way coupled FSI [20] was used for the purpose. Two field solvers, ANSYS and CFX, were coupled. To transfer loads across a dissimilar mesh interface, the nodes of one mesh (piezo) must be mapped to the local coordinates of an element in the other mesh (fluid). In a fluid-solid interaction problem, fluid nodes must be mapped to the solid elements to transfer displacements. Also, solid nodes must be mapped to the fluid elements to transfer stresses. The Multi-field solver (MFS) solution algorithm (shown in Fig. 10) must perform

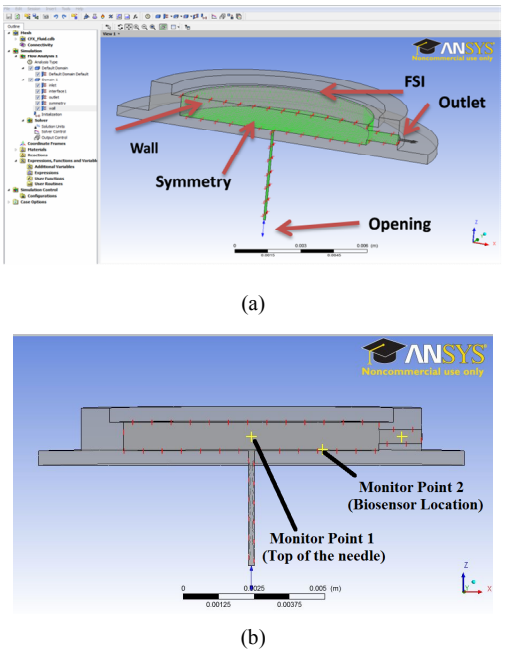

Fig. 11. (a) Boundary conditions; (b) monitor points.

two mappings for every surface to surface and volume to volume interface. ANSYS sends the displacement to ANSYS CFX. After the ANSYS CFX solver completes its computation, the hydrodynamic force is sent to ANSYS at the interface for its structural computation [21].

3.5 Boundary conditions

For the CFX analysis, following boundary conditions were imposed on the model and shown in Fig. 11(a).

3.5.1 Opening condition

As the piezo bimorph moves up, suction starts, resulting in flow of fluid in the microneedle. When the piezo bimorph moves downward, fluid may flow out through microneedle. Hence, opening boundary condition was applied at the inlet of the microneedle. At the inlet of microneedle, pressure was considered as 100 kPa, corresponding to human blood pressure. Applied boundary conditions were:

$$Uz \neq 0 \text{ (+ ve or -ve)}, \quad (1)$$

$$P = 100 \text{ kPa| microneedle inlet.} \quad (2)$$

3.5.2 Wall condition

At the bottom (Eq. (3)) of the pump chamber, on the peripheral wall of the pump chamber (Eq. (4)) and on the cylindrical surface of the outlet valve (Eq. (5)), the flow of fluid was restricted due to solid surface. Hence, Wall condition was applied:

$$Uz\,(r, \theta, 0.5) = 0, \quad (3)$$

$(0.05 \text{ mm} \leq r \leq 9 \text{ mm})$

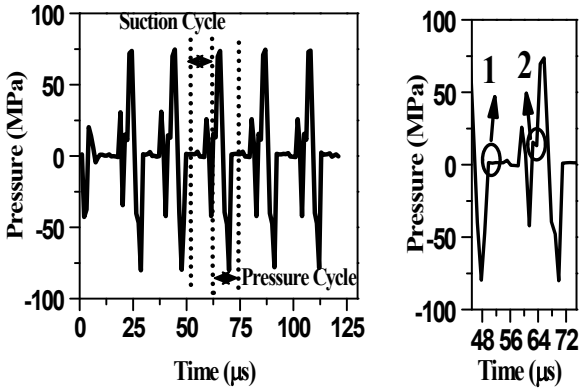

Fig. 12. (a) Pressure at top of the microneedle (monitor point 1) vs time; (b) pressure variation in one cycle.

$$U\,(4.5\text{ mm}, \theta, z) = 0, \quad (0.5\text{ mm} \le z \le 1.5\text{ mm}) \tag{4}$$

where Uz is velocity in Z direction, Ur is velocity in radial direction, r is radius of micropump chamber. At the surface of cylindrical shaped outlet valve.

$$\text{Velocity } U = 0. \tag{5}$$

3.5.3 Symmetry condition

Symmetry condition was applied along the central plane of symmetry as shown in Fig. 11(a).

3.5.4 Outlet condition

At the outlet valve, boundary condition was the outlet condition which corresponds to restriction of flow of fluid in only outward direction.

3.5.5 Interface condition

FSI boundary condition was applied at the interface of fluid region and piezo bimorph. Under this condition fluid region follows the shape of the piezo bimorph.

4. Flow analysis of micropump

For a flow analysis of the complete micropump, harmonic vibrations were generated in the piezo bimorph near its first natural frequency of 47186 Hz by applying electric field of 20 sin(2π*47186*t) at the piezo bimorph. Velocity and pressure variation for the flow was recorded at a point 0.5 mm above the top of the needle (monitor point 1) and biosensor location (monitor point 2) in the micropump chamber, as shown in Fig. 11(b). The pressure and velocity variation were recorded in time interval of 1.05963 μs. Results are summarized in Subsec. 4.1.

4.1 Pressure and velocity variation

Fig. 12(a) shows variation of pressure at monitor point 1 over six cycles (total time of 121 μs). Since the piezo bimorph was actuated at very high frequency, very high pressure of the collected fluid built up in the micropump chamber.

Fig. 12(b) shows enlarged view of the variations of pressure over a cycle. Pressure was observed to be varying from a negative value (suction) to a positive value (pressure) over a cycle. Another phenomenon observed was the presence of glitches when piezo bimorph changed its direction of deflection. Point 1 in Fig. 12(b) represents start of upward movement of piezo bimorph, i.e., suction of fluid in the pump chamber. At this time outlet valve remained closed due to reduced pressure in the fluid region. The valve remained closed during entire suction period (approximately for 10 substeps). Initially, due to negative pressure inside the flow region, pressure at monitor point 1 remained constant. During this time the flow was inside the microneedle only and did not enter the pump chamber. As soon as the flow entered inside the flow region, a non-physical sudden increase in pressure was observed.

At the start of downward movement of piezo bimorph, sudden pressure rise in monitor point 1 was observed that caused the flow of fluid towards the outlet valve instead of through the microneedle (Point 2 in Fig. 12(b)). This action generates a pressure that results in the opening of outlet valve leading to significant drop of pressure. Towards the end of pressure cycle, pressure was equalized with the outside pressure. At this point, the outlet valve closed and the collected fluid which was moving outward started moving backwards. The cycle then repeated and suction started.

Fig. 13(a) shows velocity vector plot during suction. Fluid with significant velocity can be seen entering through microneedle tip. During transition at the end of pressure cycle, since suction is causing fluid to flow-in through needle, the two streams mix in the fluid region and cause chaotic flow condition at the microneedle tip, as shown in Fig. 13(b). During pressure cycle, with the buildup of fluid pressure (about 75 MPa), the outlet valve opens. Fluid from all direction move towards outlet valve. Fig. 14 shows velocity vector plot across a horizontal plane (r-θ) passing through center of outlet valve (1mm above the bottom of pump chamber). In the near microneedle region, velocity vectors can be seen vividly moving radially outward and converging towards outlet valve. Fig. 15 shows corresponding streamline contours clearly depicting flow lines toward outlet valve. Though the flow lines are continuously converging and diverging but flow remains attached and no separation was observed.

4.1.1 Validation of simulation results

Simulation results were compared with the experimental results of Tsuchiya et al. [1] considering the same parameters. Separate simulations were carried out at 25 kHz to match with the experimental frequency. At 25 kHz frequency, deflection obtained was 272 nm as compared to 300 nm, as observed experimentally by Tsuchiya et al. Correspondingly, volume flow rate extracted using water was 14 μl/min as against 10 μl/min

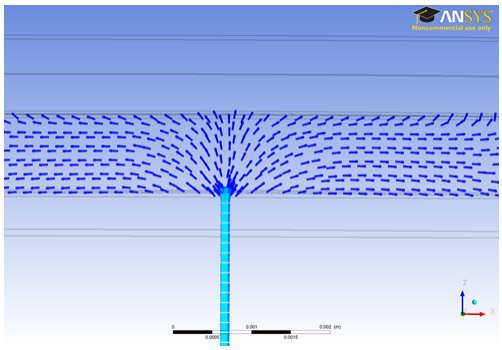

(a)

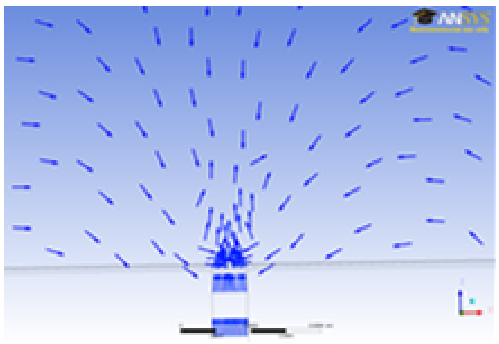

(b)

Fig. 13. Velocity vector in flow region for circular microneedle: (a) During suction cycle; (b) transition from pressure to suction cycle.

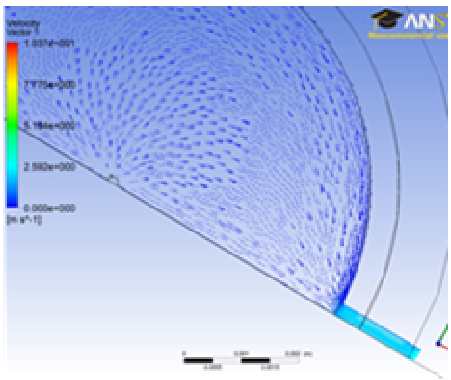

Fig. 14. Velocity vector in pump chamber at horizontal plane.

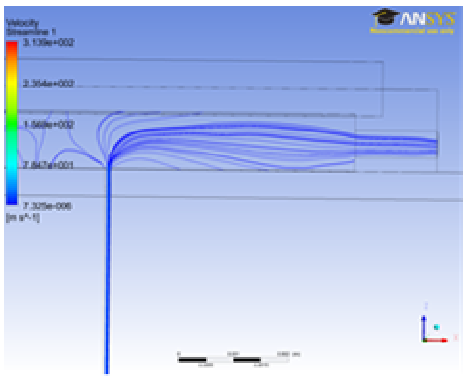

Fig. 15. Streamlines in symmetric plane at 45.60 µsec.

Table 3. Velocity and pressure comparisons.

Microneedle shape	Velocity m/s (At Top of the needle)
Circular	0.35
Octagon	0.45
Pentagon	0.25

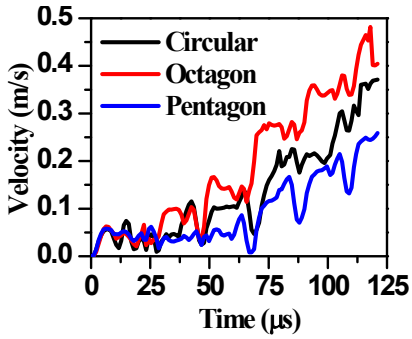

(a)

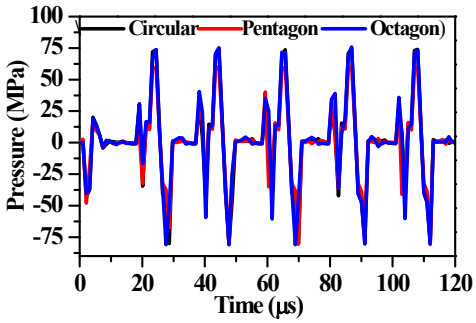

(b)

Fig. 16. (a) Velocity variations of different shapes at top of the needle (monitor point 1); (b) pressure variations at different shapes of microneedle (monitor point 1).

obtained experimentally.

4.2 Effect of shape of microneedle on flow

The flow analysis with the circular microneedle was repeated with two other shapes, pentagonal and octagonal, to observe the effect of the shape of microneedle. Velocity variations at monitor point 1 are shown in Fig. 16(a). Trends in velocity and pressure variation are almost similar for all the three shapes. Moreover, there is clear indication of highest velocity in case of octagonal shape, while lowest velocity with pentagonal shape. Since smaller velocity is desirable, hence, pentagonal shape is preferred for sensing process. Volume flow rate of water obtained at the biosensor point is 1.256 µl/s.

5. Comparison between water and blood flow

So far, flow analysis was carried out on water (Newtonian fluid) as working fluid. As the application of micropump is for

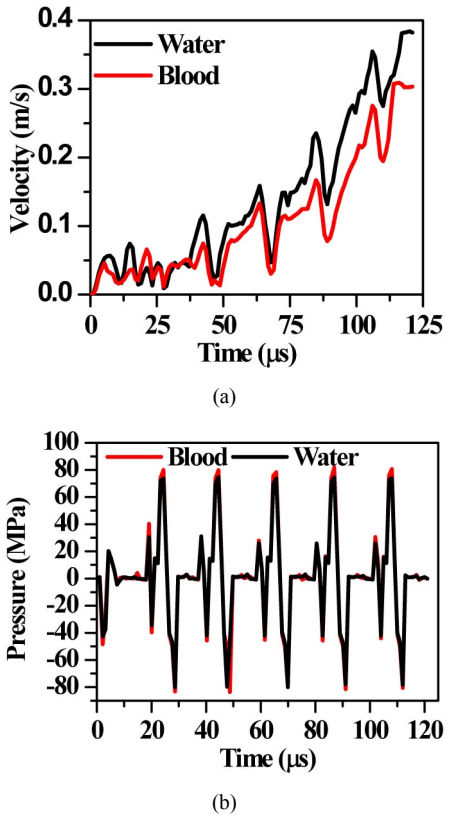

Fig. 17. Comparison of water and blood flow behavior: (a) Velocity variation; (b) pressure variation.

blood sampling (non-Newtonian fluid), a study was conducted to compare the flow behavior. The density and viscosity of water and blood are, respectively, 997 Kg/m^3, 8.9x10^{-4} Pa-s and 1060 kg/m^3, 3.5x10^{-3} Pa-s. The Reynolds number inside the microneedle for water is 38.2 and that for blood is 8.48. The range of Reynolds number for both the fluids is within creeping flow. Hence, almost similar flow behavior was observed with both water and blood as shown in Fig. 17.

6. Conclusions

A study of flow in bimorph based micropump for various shapes of the microneedle was investigated. Analysis of flow was carried out by actuating bimorph near its natural frequency to obtain the required flow through a biosensor (0.7 μl/s for blood). Following conclusions can be drawn from the study.

(a) In the transient analysis, beating phenomenon was observed, resulting in accumulation effect of fluid being sucked.

(b) Flow through micropump was of creeping flow nature, without any capillary action and separation.

(c) Optimized biosensor location can be obtained based on desired flow rate.

It can be concluded that pentagonal shape of microneedle is best for getting the desired velocity at the biosensor location.

Nomenclature

V	: Voltage
U	: Velocity
r	: Radial direction
μm	: Micro-meter
μs	: Micro seconds
MFS	: Multi field solver

References

[1] K. Tsuchiya, N. Naoyuki, U. Yasutomo and N. Eiji, Development of blood extraction system for health monitoring system, *Biomedical Microdevices,* 7 (4) (2005) 347-353, DOI:10.1007/s10544-005-6077-8.

[2] E. R. Parker, M. P. Rao, K. L. Turner, C. D. Meinhart and N. C. MacDonald, Bulk micromachined titanium microneedles, *J. of Microelectromechanical Systems,* 16 (2) (2007) 289-295, DOI 10.1109/JMEMS.2007.892909.

[3] K. Kim and J. B. Lee, High aspect ratio tapered hollow metallic microneedle arrays with microfluidic interconnector, *Microsystem Technologies,* 13 (3-4) (2008) 231-235, DOI: 10.1007/s00542-006-0221-0.

[4] J. H. Park, Y. K. Yoon, S. O. Choi, M. R. Prausnitz and M. G. Allen, Tapered conical polymer microneedles fabricated using an integrated lens technique for transdermal drug delivery, *IEEE Transactions on Biomedical Engineering,* 54 (5) (2007) 903-913, DOI 10.1109/TBME.2006.889173.

[5] N. Wilke and A. Morrissey, Silicon microneedle formation using modified mask designs based on convex corner undercut, *J. of Micromechanics and Microengineering*, 17 (2) (2006) 238.

[6] M. W. Ashraf, S. Tayyaba, A. Nisar, N. Afzulpurkar, D. W. Bodhale, T. Lomas, A. Poyai and A. Tuantranont, Design, fabrication and analysis of silicon hollow microneedles for transdermal drug delivery system for treatment of hemodynamic dysfunctions, *Cardiovascular Engineering*, 10 (3) (2010) 91-108, DOI: 10.1007/s10558-010-9100-5.

[7] A. Boonma, J. N. Roger and Y. S. Lee, Analytical modeling and evaluation of microneedles apparatus with deformable soft tissues for biomedical applications, *Computer-Aided Design and Applications*, 10 (1) (2013) 139-157.

[8] C. G. Li, K. Lee, C. Y. Lee, M. Dangol and H. Jung, A minimally invasive blood‐extraction system: Elastic self-recovery actuator integrated with an ultrahigh-aspect-ratio microneedle, *Advanced Materials*, 24 (33) (2012) 4583-4586.

[9] N. Nakanishi, H. Yamamoto, K. Tsuchiya, Y. Uetsuji and E. Nakamachi, Development of wearable medical device for Bio-MEMS, *Microelectronics, MEMS, and Nanotechnology,* (2005) 60360P-60360P, International Society for Optics and Photonics, DOI:10.1117/12.638162.

[10] C. G. Li, C. Y. Lee, K. Lee and H. Jung, An optimized hollow microneedle for minimally invasive blood extraction, *Biomedical Microdevices*, 15 (1) (2013) 17-25, DOI: 10.1007/s10544-012-9683-2.

[11] J. Gupta, S. S. Park, B. Bondy, E. I. Felner and M. R. Prausnitz, Infusion pressure and pain during microneedle injection into skin of human subjects, *Biomaterials,* 32 (28) (2011) 6823-6831.

[12] S. Henry, D. V. McAllister, M. G. Allen and M. R. Prausnitz, Micromachined needles for the transdermal delivery of drugs, *Micro Electro Mechanical Systems, The Eleventh Annual International Workshop* (1998) 494, DOI: 10.1109/MEMSYS.1998.659807.

[13] Y. Bar-Cohen and Z. Chang, Piezoelectrically actuated miniature peristaltic pump, *SPIE's 8th Annual International Symposium on Smart Structures and Materials* (2001) 425-432.

[14] F. Bin, G. Song and F. Hussain, Simulation of a piezoelectrically actuated valveless micropump, *Smart Structures and Materials,* 14 (2) (2004) 400, DOI 10.1088/0964-1726/14/2/014.

[15] D. H. Ha, V. P. Phan, N. S. Goo and C. H. Han, Three-dimensional electro-fluid-structural interaction simulation for pumping performance evaluation of a valveless micropump, *Smart Materials and Structures*, 18 (10) (2009) 104015.

[16] S. Warisawa, K. Tsuchiya, V. K. Gupta, T. Sheorey and P. Tandon, Design and analysis of a micro pump for wearable blood sampling system, *2012 ASME-ISPS /JSME-IIP Joint International Conference on Micromechatronics for Information and Precision Equipment (MIPE2012),* June 18-20 (2012) Santa Clara, California, USA.

[17] S. D. Thorat and A. B. K. Patil, Study of performance analysis of reciprocating pumps using CFD, *Ird-India Advance Physics Letter*, 4 (1) (2015) 40-46, ISSN (Print): 2319-3182.

[18] R. N. Rajeswari and P. Malliga, Analytical approach for optimization design of MEMS based microneedles in drug delivery system, *J. of Mechanical Science and Technology*, 29 (8) (2015) 3405-3415.

[19] X. He, L. Xu, X. Zhang and S, Yang, A bidirectional valveless piezoelectric micropump with three chambers applying synthetic jet, *J. of Mechanical Science and Technology*, 30 (9) (2016) 4015-4022.

[20] F. K. Benra, H. J. Dohmen, J. Pei, S. Schuster and B. Wan, A comparison of one-way and two-way coupling methods for numerical analysis of fluid-structure interactions, *J. of Applied Mathematics* (2011) V-2011, Doi:10.1155/2011/853560.

[21] *Ansys12.1® help document*, ANSYS Multi-field solver Solution Procedure.

Rakesh Kumar Haldkar received the B.E. in Mechanical Engineering from the Gyan Ganga Institute of Technology and Sciences Jabalpur (MP), India, in 2008, and Master of Technology (M.Tech.) from the PDPM Indian Institute of Information Technology Design and Manufacturing (IIITDM) Jabalpur (MP) India, in 2011. He is a Ph.D. student in PDPM IIITDM Jabalpur. His current research areas are piezo based micropump and energy harvesting.

Vijay Kumar Gupta is currently a Professor at PDPM IIITDM Jabalpur. He received Ph.D. from Indian Institute of Technology Bombay in Smart Structures. His research interests include mechanical vibrations, smart structures, MEMS, mechatronics, robotics and finite element analysis.

Tanuja Sheorey is currently a Professor at PDPM IIITDM Jabalpur. She received the B.E. in Mechanical Engineering in 1985 from Government Engineering College, Jabalpur (MP) India, Master of Technology (M.Tech) from M.A. National Institute of Technology, Bhopal in 1988 and Ph.D. in 2002 from Indian Institute of Technology, Kanpur. Her research works are on computational fluid dynamics, and micro-fluidic devices**.**